



Published in final edited form as:

Nat Microbiol. 2019 October ; 4(10): 1737–1749. doi:10.1038/s41564-019-0470-1.

IFN-I and IL-22 mediate protective effects of intestinal viral infection

Jessica A Neil¹, Yu Matsuzawa-Ishimoto¹, Elisabeth Kernbauer-Hözl¹, Samantha L Schuster¹, Stela Sota^{1,2}, Mericien Venzon^{1,2}, Simone Dallari¹, Antonio Galvao Neto³, Ashley Hine^{4,5}, David Hudesman⁵, P'ng Loke⁴, Timothy J Nice⁶, Ken Cadwell^{1,4}

¹Kimmel Center for Biology and Medicine at the Skirball Institute, New York University School of Medicine, New York, New York 10016, USA

²Sackler Institute of Graduate Biomedical Sciences, New York University School of Medicine, New York, New York 10016, USA

³Department of Pathology, New York University School of Medicine, New York, New York 10016, USA

⁴Department of Microbiology, New York University School of Medicine, New York, New York 10016, USA

⁵Department of Medicine, Division of Gastroenterology, New York University School of Medicine, New York, New York 10016, USA

⁶Department of Molecular Microbiology and Immunology, Oregon Health and Science University, Portland, OR, USA

Abstract

Products derived from bacterial members of the gut microbiota evoke immune signaling pathways from the host that promote immunity and barrier function in the intestine. How immune reactions to enteric viruses support intestinal homeostasis is unknown. Recently, we demonstrated that infection by murine norovirus (MNV) reverses intestinal abnormalities upon depletion of bacteria, indicating that an intestinal animal virus can provide cues to the host that are typically attributed to the microbiota. Here, we elucidate mechanisms by which MNV evokes protective responses from

Users may view, print, copy, and download text and data-mine the content in such documents, for the purposes of academic research, subject always to the full Conditions of use:http://www.nature.com/authors/editorial_policies/license.html#terms

To whom correspondence should be address: Ken Cadwell, Ph.D. New York University School of Medicine, ACLS-WT 409, 430 East 29th Street, New York, NY, 10016, USA. Telephone: (212) 263-8891. Fax: (212) 263-5711. kencadwell@med.nyu.edu.

Author Contributions

J.A.N. and K.C. formulated the original hypothesis and designed the study. J.A.N. performed the experiments and analysis, and received assistance from E.K. (DSS experiments), S.S. (in vitro MNV responses) and Y.M-I. (organoids). S.L.S. and M.V. processed and analyzed the samples for 16S rRNA sequencing. A.G.N performed the histopathology analysis. P.L., D.H., and A.H provided the human colon biopsies. S.D. performed sorting of IECs. T.N. provided the cDNA clones of MNV and advice. J.A.N. and K.C. wrote the manuscript. All authors commented on the manuscript, data and conclusions.

Data Availability

The data that support the findings of this study are available from the corresponding author upon request. FASTQ files corresponding to the RNA-seq and 16S rRNA sequencing have been deposited in a public database (RNA-seq accession no. GSE129384, 16S accession no. PRJNA532632).

Competing Financial Interests

K.C. has consulted for PureTech Health and AbbVie Inc. and is an inventor on U.S. patent application 62/608,404.

the host. We identify an important role for the viral protein NS1/2 in establishing local replication and a type I interferon (IFN-I) response in the colon. We further show that IFN-I acts on intestinal epithelial cells to increase the proportion of CCR2-dependent macrophages and IL-22 producing innate lymphoid cells (ILCs), which in turn promote pSTAT3 signaling in intestinal epithelial cells and protection from intestinal injury. Additionally, we demonstrate that MNV provides a striking IL-22 dependent protection against early life lethal infection by *Citrobacter rodentium*. These findings demonstrate novel ways in which a viral member of the microbiota fortifies the intestinal barrier during chemical injury and infectious challenges.

INTRODUCTION

The microbiome includes intestinal bacteria that contribute to the development of the immune system, defend against opportunistic infections, and impact the development of autoimmune and inflammatory disease. Bacteriophages, animal viruses, and endogenous viral elements that represent the virome are also numerous, diverse, and prevalent in humans and model organisms¹. Alterations in the composition of the enteric virome have been observed in various pathological conditions, suggesting that the presence or absence of certain viruses in the gastrointestinal tract contribute to disease development². Although many animal viruses have been detected in intestinal specimens, insight into mechanisms by which enteric viruses influence host physiology beyond their roles as pathogens is lacking. An understanding of viral and host factors involved in establishing mutually beneficial relationships could influence the design and implementation of microbiome-based therapies, which currently focus on exploiting bacterial communities.

Studies with murine norovirus (MNV) provide direct evidence that viruses can function similarly to the bacterial members of the microbiome. MNV is a single-stranded RNA virus that frequently establishes a persistent asymptomatic gastrointestinal infection in mice. Like commensal bacteria, MNV induces or exacerbates intestinal inflammation in genetically susceptible backgrounds³⁻⁵. In mice with mutation in the autophagy gene *Atg16L1*, a model of the inflammatory bowel disease (IBD) Crohn's disease, we showed that MNV infection triggers structural defects in small intestinal Paneth cells similar to patients harboring the disease-associated variant of *ATG16L1*^{3,6}. MNV-infected *Atg16L1* mutant mice also display increased mortality following chemical injury to the intestine by dextran sodium sulfate (DSS)^{3,7}. Conversely, we demonstrated in wild-type (WT) antibiotics (ABX)-treated and germ-free (GF) mice that the same MNV strain restores intestinal morphology and lymphocyte differentiation that are defective due to the absence of bacteria⁸. In addition, and in stark contrast to *Atg16L1* mutant mice, MNV protects ABX-treated mice from DSS-induced mortality⁸. Subsequently, other groups showed that MNV enhances colonization resistance against vancomycin-resistant enterococcus (VRE) after ABX treatment and reduces lung injury following infection with *Pseudomonas aeruginosa*^{9,10}. This property of MNV, where infection can be beneficial in certain situations yet induces disease in a susceptible background, is reminiscent of the complex symbiotic relationship between host and the bacterial microbiota.

Endogenous viruses and synthetic viral RNA were shown to protect against DSS through production of type I interferon (IFN-I) by dendritic cells (DCs)^{11,12}. Similarly, we demonstrated that MNV-mediated protection against DSS in ABX-treated mice is dependent on the IFN-I receptor (IFNAR1), implicating this conserved antiviral pathway in the protective effects of viral infection⁸. *Ifnar1*^{-/-} mice that were not treated with ABX, and thus harbor an intact bacterial microbiota, were similar to WT mice and resistant to DSS under the same conditions. These findings raise the possibility that virus-mediated protection occurs through a mechanism that is distinct from the way an intact bacterial microbiota fortifies the barrier, which we examine here.

RESULTS

Protection from chemical injury is dependent on sequence variation in NS1/2.

We previously showed that the CR6 strain of MNV strain confers greater protection of ABX-treated mice from DSS compared to the CW3 strain⁸. Although MNV CR6 and CW3 share ~95% amino acid sequence identity, they display significant differences in their virulence. The VP1 major capsid protein of MNV CW3 accounts for the ability of this strain to cause lethality when introduced into immunocompromised *Stat1*^{-/-} mice¹³⁻¹⁵. The less virulent CR6 strain evades recognition by lymphocytes to establish persistent infection¹⁶, which is attributed to sequence variation in NS1/2¹⁷. We used recombinant cDNA clones of MNV in which the VP1 and NS1/2 regions were swapped between CR6 and CW3 (Fig. 1a) to determine which of these factors contribute to protection from DSS.

First, we used GF mice to verify our previous observations made in ABX-treated mice. GF mice infected with MNV CR6, but not CW3, displayed survival following administration of DSS to levels similar as conventional mice, indicating that the CR6 strain has the ability to compensate for the complete absence of bacteria (Fig. 1b and Sup. Fig. 1a). Although no chimeric virus was able to induce the same level of protection as CR6, we observed significant differences. Sequence variation in VP1 did not contribute to protection as the CR6 mutant harboring VP1 from CW3 (CR6.VP1^{CW3}), but not the converse (CW3.VP1^{CR6}), improved the survival of GF mice (Fig. 1c). In contrast, the CW3 mutant harboring NS1/2 from CR6 (CW3.NS1/2^{CR6}) gained the ability to promote survival, while the CR6 mutant harboring NS1/2 from CW3 (CR6.NS1/2^{CW3}) lost this ability (Fig. 1d). We previously showed that protection against DSS correlates with the ability of MNV to restore the width of small intestinal villi in bacterially-depleted mice⁸. We found that the strains that enhanced survival during DSS treatment (MNV CR6, CR6.VP1^{CW3}, and CW3.NS1/2^{CR6}) increased the villus width of GF mice (Fig. 1e and 1f). Therefore, NS1/2 contributes to the differential response to MNV CR6 and CW3 infection.

We detected all virus strains in the stool at day 10 post-infection indicative of productive infection, albeit at lower levels than conventional mice consistent with the role of bacteria in promoting MNV infection^{8,18,19}. However, the parental CR6 strain replicated to higher titers (Fig. 1g). We did not detect any correlation between extra-intestinal spread and survival following DSS treatment (Sup. Fig. 1b). A more efficient intestinal infection could explain why GF mice infected with CR6 display the highest degree of survival, even when compared with CW3.NS1/2^{CR6} infection. Importantly, CW3.NS1/2^{CR6} (which protects against DSS)

and the original CW3 strain (which does not protect) display similar degree of shedding indicating that additional factors are important for determining the effect of MNV infection on intestinal injury.

NS1/2 contributes to IFN-I signaling and proliferation of colonic epithelial cells.

NS1/2 sequence variation is associated with persistence in the colon of conventional mice^{17,20}. We hypothesized that the chimeric viruses have differences in the ability to replicate in the colon during injury and drive local viral RNA sensing that is important for the protective IFN-I response. Consistent with this possibility, we observed a correlation between the amount of MNV RNA from the chimeric viruses and expression of the representative IFN-stimulated genes (ISGs) *OasL2*, *Mx2* and *Isg15* in the colonic tissue of virally-infected GF mice treated with DSS (Fig. 2a). Although previously shown to primarily infect leukocytes, recent findings indicate that MNV also infects intestinal epithelial cells (IECs), especially tuft cells^{20,21}. Only CR6 and CW3.NS1/2^{CR6} genomes were detectable in sorted IECs and lamina propria leukocytes (LPLs) indicating that CW3 and CR6.NS1/2^{CW3} are unable to persist in the colon following DSS treatment (Fig. 2b). The presence of viral RNA in IECs rather than LPLs was a better indicator of ISG expression, and IFN-I expression (*Ifnb1*) was detectable in LPLs but not IECs (Fig. 2c and Sup. Fig. 1c). These results suggest that, even though the epithelial tropism of MNV is important for persistence in the local niche, immune cells are likely the main producers of IFN β and IECs are the responding cells under these conditions.

Mice deficient in *Irgm1*, a negative regulator of IFNAR1 signaling, display enhanced wound healing due to increased IEC proliferation²². Similarly, we found that GF mice infected with MNV CR6 and CW3.NS1/2^{CR6}, but not those infected by MNV CW3 or CR6.NS1/2^{CW3}, showed increased staining of the proliferation marker Ki67 in the colon (Fig. 2d). The IFN-I response to MNV is dependent on recognition of viral RNA by cytosolic sensors that signal through the adaptor molecule MAVS^{23–25}. Unlike *Mavs*^{+/+} controls, MNV CR6 infection of ABX-treated *Mavs*^{-/-} mice did not induce ISGs, protect against DSS, or restore the width of small intestinal villi despite productive viral replication (Sup. Fig. 2a–d). MNV CR6 infection of bone marrow-derived DCs induced MAVS-dependent expression of *Ifnb1* and *Mx2* (Sup. Fig. 2e). Conversely, MNV CR6 induced *Mx2* expression without detectable *Ifnb1* in both *Mavs*^{+/+} and *Mavs*^{-/-} intestinal organoids, a 3D cell culture in which epithelial lineages are differentiated from primary progenitor cells (Sup. Fig. 2f). These data support a role for MAVS-induced IFN-I production by leukocytes in response to MNV persistence in the colon, which is associated with protective epithelial proliferation.

Protection from DSS by MNV is dependent on IL-22.

We and others have shown that MNV infection increases IL-22-producing group 3 innate lymphoid cells (ILC3s) and IFN γ ⁺ T cells in GF or ABX-treated mice^{8,9}. MNV CR6 retained the ability to improve the survival of ABX+DSS-treated IFN- γ receptor (*Ifngr*^{-/-}) mice, but was unable to protect similarly-treated *Il22*^{-/-} mice (Fig. 3a–c). *Il22*^{-/-} mice that received DSS without ABX displayed 100% survival, indicating that IL-22 is dispensable at this particular dose and duration of DSS treatment when intestinal bacteria are intact, and that this cytokine is especially necessary to overcome the heightened sensitivity to injury

when bacteria are depleted. The loss of protection in *Il22*^{-/-} mice could not be explained by lower intestinal virus levels (Fig. 3e). Increased villus width was observed following CR6 infection in ABX-treated WT and to a lesser extent *Ifngr*^{-/-} mice, but not *IL-22*^{-/-} mice (Fig. 3d). These observations support the idea that widening of villi reflects an increase in leukocytes and IEC proliferation downstream of an immune response to local viral replication.

Next, we examined whether MNV induces phosphorylation of STAT3 (pSTAT3) in the colon because activation of this transcription factor downstream of IL-22 signaling mediates wound repair following DSS treatment²⁶. We detected an IL-22 dependent increase in pSTAT3⁺ cells in the colon upon infection with MNV CR6, whereas the positive control pSTAT1 (induced by IFN-I, IFN-λ, and IFN-γ) was detectable in all conditions (Fig. 3f-h). Interestingly, we found that MNV was also unable to induce pSTAT3 staining in the colon of *Ifnar1*^{-/-} mice (Fig. 3h). MNV CR6 infection still induced significant ISG expression in *Il22*^{-/-} mice (Sup. Fig. 3a), indicating that IFN signaling is not dependent on IL-22. MNV CR6 infection increased the proportion and absolute numbers specifically of IL-22-producing ILCs in the colonic lamina propria in ABX+DSS-treated WT but not *Ifnar1*^{-/-} mice (Fig. 3i-j, Sup. Fig. 3b-c and 3e). Viral infection increased IFNγ⁺ CD4⁺ T cell populations (but not IL-22⁺ or IL-13⁺ CD4⁺ T cells) in an IFNAR1-dependent manner (Fig. 3i and 3j and Sup. Fig. 3d and 3f), but our earlier results (Fig. 3b) show that IFNγ was not involved in protection from injury. MNV CR6 evoked similar responses in GF mice following DSS (Sup. Fig 3g and 3h). Also, IL-22 secretion in colonic explants and pSTAT3 staining in colonic tissue sections were increased in GF mice infected by MNV CR6 (Sup. Fig. 3i and 3j). Together, these results indicate that MNV CR6 increases colonic IL-22 following intestinal damage.

Activation of ILC3s following bacterial infection of the colon is dependent on recruitment of CCR2⁺ monocytes²⁷. We found that MNV CR6 infection did not increase the proportion of IL-22⁺ ILCs in the colon of ABX-treated *Ccr2*^{-/-} mice, indicating that similar mechanisms are necessary for virus-mediated activation of ILC3s (Fig. 4a). Despite equivalent or higher viral burden compared with *WT* mice, MNV CR6 induced minimal protection from DSS injury in ABX-treated *Ccr2*^{-/-} mice (Fig. 4b and 4c). We observed an increase in several CCR2-dependent MHCII⁺ myeloid populations in the colon following infection with MNV CR6 (Sup. Fig. 4a and Fig. 4d). Among these infiltrating cells, MNV-induced increases in CD11b^{low}CD11c⁺CD103⁻ cells was observed in GF and ABX-treated *WT* mice but not ABX-treated *Ifnar1*^{-/-} mice (Fig. 4e and Sup. Fig. 4b). Other MHCII⁺ populations were not dependent on IFN-I signaling, and recruitment of all subsets following infection remained intact in *Il22*^{-/-} mice (Fig. 4e). Therefore, MNV-mediated protection from injury is associated with IFN-dependent alterations to myeloid populations upstream of IL-22 expression by ILC3s.

IFN-I signaling in IECs is required for protection.

Although *Ifnar1* deletion in IECs alters the composition of the bacterial microbiota²⁸, other studies have shown that IECs are unresponsive to IFN-I and implicate a dominant role for IFN-λ signaling in inhibiting enteric RNA viruses^{19,29-31}. In contrast to *Ifnar1*^{fl/fl} control

mice, MNV infection of ABX-treated *Ifnar1^{fl/fl}*;villin-Cre mice in which *Ifnar1* is deleted in IECs (*Ifnar1^{IEC}*) did not enhance survival following DSS injury or restore villi width (Fig. 5a–c). We did not observe an IEC-specific role for IFNAR1 in restricting MNV burden (Fig. 5d). The ability of MNV CR6 to induce pSTAT3 staining was eliminated in *Ifnar1^{IEC}* but not *Ifnar1^{fl/fl}* mice (Fig. 5e). Recombinant IFN β induced *Mx2* expression in human and mouse intestinal organoids (Fig. 6a–c), confirming that IECs can directly respond to IFN-I. According to our model, STAT3 is activated by IL-22 directly and IFN-I indirectly during MNV infection. We found that IL-22, but not IFN β , induced pSTAT3 and REG3 β in organoids (Fig. 6d, 6e and Sup. Fig. 6). These findings show that IECs respond to IFN-I, and that STAT3 phosphorylation is an independent event. MNV-induced increases in IL-22⁺ and IFN γ ⁺ ILCs and MHCII⁺CD11b^{low}CD11c⁺CD103⁻ cells were absent in *Ifnar1^{IEC}* mice (Fig. 6f–g and Sup. Fig. 4c–d). We then performed RNA-Seq analysis on sorted IECs from *Ifnar1^{fl/fl}* and *Ifnar1^{IEC}* mice following DSS, with or without viral infection. MNV CR6 infection led to increased expression of genes representing cell cycle regulation and DNA damage response pathways in a manner dependent on epithelial IFNAR1 (Fig. 6h). This IFNAR-dependent gene expression pattern is consistent with MNV-induced IEC proliferation (Fig. 2d) and is remarkably similar to a recently described IL-22 induced transcriptional response that prevents genotoxic damage to epithelial stem cells in the colon³². Together, these data indicate that IFNAR signaling in the epithelium mediates the beneficial effect of MNV infection, and decouples the role of IFN-I in antiviral versus injury responses.

MNV protects against enteric bacterial infection during development.

The gastrointestinal tract becomes exposed to diverse animal viruses over time following birth³³. It is unclear how the presence of these viruses affect disease caused by enteric bacterial pathogens, which are also a common occurrence during childhood. To examine the consequence of coinfection, 3-week old WT mice were challenged with the Gram-negative bacterial pathogen *Citrobacter rodentium*, with or without concurrent MNV CR6 infection. In the absence of the virus, WT mice failed to grow and succumbed to *C. rodentium* infection, whereas almost all the MNV CR6-infected mice survived and gained weight (Fig. 7a). MNV CR6 did not provide any benefit to 3-week old *Il22^{-/-}* mice (Fig. 7b). Next, we took advantage of the observation that lymphocyte-deficient *Rag1^{-/-}* mice have a compensatory increase in IL-22 producing ILC3s during a similar developmental period as the above coinfection model³⁴. We hypothesized that this increase in ILC3s would serve a similar purpose as MNV infection, and thus, *Rag1^{-/-}* mice will no longer be dependent on MNV for survival during *C. rodentium* infection. Indeed, *Rag1^{-/-}* mice were protected from bacterial infection irrespective of MNV infection, which was associated with an overall increase in ILCs (Sup. Fig. 5a–b). Therefore, enhancing IL-22⁺ ILC3s through viral infection or genetically is associated with protection against secondary bacterial infection in juvenile animals.

IL-22 is more important for reducing intestinal inflammation rather than intestinal *C. rodentium* burden in adult mice³⁵. Consistent with this observation, MNV CR6 infection of WT mice led to modest or no reduction in bacterial burden (Fig. 7c–e). Furthermore, similar numbers of *C. rodentium* were recovered from the stool of MNV-infected WT and *Il22^{-/-}*

mice. Instead, we observed that MNV CR6 infection reduced intestinal pathology in an IL-22 dependent manner (Sup. Fig. 5c). Protection from *C. rodentium* infection was independent of MNV strain, as CW3-infected WT mice showed increased survival and weight gain (Sup. Fig. 5d). Protection from *C. rodentium* infection was also maintained in *Ifnar1*^{-/-} mice (Sup. Fig. 5e). Thus, sequence variation in NS1/2 and IFNAR1 signaling do not contribute to protection from bacterially-induced injury.

It is possible that MNV protects young mice by accelerating the development of the microbiota because the compositional shift in intestinal bacterial communities that occurs during neonatal development is key to *C. rodentium* resistance³⁶. However, we did not detect significant changes in the gut microbiota due to MNV infection or absence of IL-22 (Sup. Fig. 5f). Instead, MNV-mediated protection from *C. rodentium* was associated with a general increase in the proportion of CD4⁺ and CD8⁺ T cells in the colon, which was not observed in MNV-infected *Il22*^{-/-} mice (Fig. 7f). In addition, MNV CR6 increased the proportion of IFN γ -expressing CD8⁺ T cells and ILCs in an IL-22 dependent manner, and similar to the DSS model, the presence of the virus was associated with IL-22⁺ ILCs (Fig. 7g and 7h).

DISCUSSION

The bacterial members of the gut microbiota acquired during development promote the maturation of the immune system and intestinal barrier. This mutualistic host-microbiota relationship can be disrupted in adulthood by ABX, diet, or other factors that alter bacterial community structures. Thus, tremendous effort has been placed in understanding the mechanistic basis of this relationship, and clinical trials are attempting to remodel the microbiota in diseased individuals by transplanting isolated microbes or feces from healthy donors. Despite accumulating evidence of the presence of a dynamic enteric virome that begins to take shape after birth³³, it is unknown how intestinal viruses impact the resilience of the intestinal barrier to damage caused by environmental agents. Using two distinct models, we show that MNV infection improves the outcome of intestinal injury through IL-22.

In the chemical injury model, we demonstrate that compensation for the absence of beneficial bacteria by MNV is associated with the NS1/2 region of the viral genome. NS1/2 from mouse and human noroviruses binds the host molecule VAMP-associated protein A (VAPA), which potentially mediates membrane remodeling during viral replication³⁷⁻³⁹. NS1/2 is structurally disordered and subject to cleavage, suggesting that it can adopt additional conformations with alternate functions that are currently unknown⁴⁰. NS1/2 from the protective MNV CR6 strain confers the ability to replicate and persist in colonic IECs, leading to a local IFN-I response that is likely downstream of MAVS-dependent IFN β production in neighboring immune cells, although we cannot rule out an epithelial contribution of IFN β . Our extensive analysis of *Ifnar1*^{IEC} mice indicate that IECs are the IFN-responding cell type.

We further found that MNV induces IL-22 producing ILC3s in an IFNAR1 and CCR2-dependent manner. Unlike IFN- λ which acts on neutrophils to protect against DSS⁴¹, we

identified a role for IFN-I acting on IECs to mediate recruitment or activation of CCR2-dependent cells during MNV infection. Recently, we showed that enhanced IFN-I signaling due to autophagy inhibition in IECs alters the function of CCR2-dependent monocytes⁴². Thus, it is also plausible that augmenting IFN-I signaling through MNV CR6 infection also induces functional changes to these populations. A role for macrophages in the activation of ILC3 has been previously demonstrated following *C. rodentium* infection²⁷. Therefore, we hypothesize that alterations in proportions and potentially function of macrophage populations, through IFNAR1-mediated responses in IECs, affects the ability of these cells to promote IL-22 production by ILC3s.

MNV-mediated protection of young mice from *C. rodentium* is IL-22 dependent as well. The mechanism is distinct from another study which reported that MNV confers resistance to VRE in ABX-treated adult mice involving a virus-dependent reduction in bacterial colonization⁹. VRE is a Gram-positive bacterium that is sensitive to antimicrobial REG molecules produced in response to IL-22, whereas other functions such as epithelial repair may be more important for protecting against Gram-negative bacteria such as *C. rodentium*, especially in young mice. Recently it was shown that MNV recruits CCR2-dependent monocytes to the MLN in an IFNAR1-independent manner to support systemic persistence⁴³. Although we identified a subset of myeloid cells that were IFNAR1 dependent, this was not universal across all subsets. Therefore, unlike the DSS model, accumulation of IFNAR1-independent macrophages may be sufficient to provide protection following *C. rodentium* infection, which would explain why IFNAR1 is dispensable and MNV CW3 is able to provide protection. Due to its increased virulence compared with other strains, infection of mice with MNV CW3 has been used as a surrogate for pandemic human norovirus GII.4 strains. Given that up to 30% of asymptomatic infants and children are positive for norovirus RNA in the stool⁴⁴, concurrent infection with bacterial pathogens is likely commonplace. Our results raise the possibility that underlying norovirus infections may have a protective role when the virus is not evoking diarrheal disease.

The inter-strain diversity between human noroviruses is far greater than the sequence differences between MNV strains, yet little is known about how different noroviruses impact the mucosal immune system of the human gut. This lack of knowledge applies to other enteric viruses as well. Elegant work combining observations in mice and humans implicate reoviruses and noroviruses in celiac disease onset in a viral strain-dependent manner^{45,46}. CMV can reactivate in the gastrointestinal tract and contribute to IBD flares, but was shown to enhance epithelial turnover in mice, which presumably improves resistance to injury²². These observations resemble some aspects of our findings with MNV showing that an intestinal virus can be beneficial or adverse depending on the strain and properties of the host. Finally, we wish to note that few studies investigating the effect of the bacterial microbiota exclude the possibility that results are driven by the presence of MNV or other enteric viruses such as astroviruses common in mouse facilities. We suggest that the host immune response to enteric viral infections requires attention beyond its antiviral function and needs to be considered in microbiota studies.

MATERIALS AND METHODS

Mice

GF mice on a C57BL/6J background were bred and maintained in flexible-film isolators in the New York University (NYU) School of Medicine Gnotobiotics Animal Facility. Absence of fecal bacteria was confirmed monthly as before⁸. For experiments, GF mice were housed in Techniplast Bioexclusion cages with access to sterile food and water. Conventional C57BL/6J WT, *Ifnar1*^{-/-}, *Ifngr*^{-/-} *Ccr2*^{-/-}, *Mavs*^{-/-}, *Rag1*^{-/-}, *Ifnar1*^{fl} and *Villin-cre* mice were purchased from Jackson Laboratories. *IL22*^{-/-} mice were provided by Sergei Koralov (NYUMC, USA). *Ifnar1*^{fl} mice were bred to *Villin-cre* mice to produce *cre*^{+/-} and *cre*^{-/-} littermates. *Mavs*^{-/-} mice on a B6129SF2/J background were bred to C57BL/6J mice to produce *Mavs*^{+/-} mice that were crossed to each other to produce *Mavs*^{-/-} and *Mavs*^{+/+} littermates. All other knockout strains were on the C57BL/6J background, and C57BL/6J mice were used as WT controls. All mice were bred onsite in an MNV and *Helicobacter*-negative specific-pathogen free (SPF) animal facility. For DSS experiments, randomly assigned age (8–10 weeks) and gender-matched mice were used in which MNV-infected mice were compared with uninfected littermates to control for potential microbiota differences between mice originating from different breeding pairs. For *Citrobacter rodentium* experiments, age-matched 12–14-day-old litters were used that were generated from 2 pregnant dams that were co-housed and the subsequent litters separated approximately 2–4 days prior to infection with MNV. Dams were littermates from the previous generation. All young mice were weighed daily throughout the experiment. Sample size for animal experiments was chosen based on prior data generated in the laboratory. All animal studies were performed according to protocols approved by the NYU School of Medicine Institutional Animal Care and Use Committee (IACUC).

Antibiotics and DSS treatment

For ABX treatment, mice were given filter-sterilized water containing ampicillin (1 g l⁻¹; American bioanalytical), vancomycin (0.5 g l⁻¹; Sigma), neomycin (1 g l⁻¹; Sigma), metronidazole (1 g l⁻¹; Sigma) and 1% sucrose (Sigma). ABX-containing water was replaced at least once a week. Mice were treated with this ABX cocktail for at least 10 days prior to infection. Mice were given 3% DSS (TdB consultancy) with or without the ABX cocktail in their drinking water for 6 days and then received regular or ABX-containing drinking water for the remainder of the experiment. GF mice were given 3% DSS in filter-sterilized water for 5 days. Mice were monitored daily for survival.

MNV and bacterial inoculation

Plasmids for chimeric MNV strains were previously described¹⁷. Two viruses were on a CR6 backbone containing the indicated gene from CW3: CR6.VP1^{CW3} and CR6.NS1/2^{CW3}. Two viruses were on a CW3 backbone containing the indicated gene from CR6: CW3.VP1^{CR6} and CW3.NS1/2^{CR6}. Chimeric viruses, CW3 and CR6 were prepared and titrated as described previously⁸. Mice were infected orally by pipette with 3 × 10⁶ pfu resuspended in PBS (Corning). *C. rodentium* DBS100 was grown overnight in Luria-Bertani broth with shaking at 37°C and diluted 1:100 followed by an additional 4 hours of growth

until bacteria were at an optical density of 2. Mice were gavaged with 2×10^7 cfu. Bacterial inocula were determined by serial dilution plating on MacConkey plates.

Detection of infectious MNV and *Citrobacter rodentium* in organs

Stool, 2cm ileum, 2cm of ascending colon, liver, spleen and MLN were harvested from MNV-infected mice at 10 dpi. Organs were weighed and homogenized in serum-free DMEM (Corning). Titers of MNV were determined by plaque assay as previously described⁸. Titers are shown as pfu/g or pfu/cm. Stools, liver and spleen were harvested from *C. rodentium*-infected mice at 6 dpi. Organs were weighed and homogenized in PBS and serial dilutions plated onto MacConkey plates. Titers are shown as cfu/g.

Organoid culture

Murine small intestinal and colonic organoids were cultured as described previously⁷. At day 5 (SI) or day 3 (colon) organoids were stimulated with either 500 U/ml of IFN β (PBL Assay Science), 5 ng/ml of IL-22 (Biolegend) or left unstimulated. For RNA extraction and immunofluorescence, the organoids were stimulated for 24 or 48 h. For detection of STAT3 phosphorylation, organoids were stimulated for 2h. For human organoids, pinch biopsies were obtained from the colon of adult IBD patients undergoing surveillance colonoscopy using 2.8 mm standard biopsy forceps, after approval by the New York University School of Medicine Institutional Review Board. All tissue was isolated from non-inflamed regions of the colon. Intestinal fragments were incubated in Gentle Cell Dissociation Reagent (Stemcell Technologies) on ice for 30 minutes followed by vigorous pipetting to isolate crypts. Crypt were embedded in Corning Matrigel Growth Factor Reduced Basement Membrane Matrix (Corning), and cultured with human IntestiCult Organoid Growth Medium (Stemcell Technologies). The culture medium was changed every 2–3 days. Human organoids were stimulated with 500 U/ml IFN β (R&D systems) or left unstimulated for 48 h.

Culture of BMDCs and intestinal organoids in the presence of MNV

Murine BMDCs were derived from bone marrow cells stimulated with 20ng/ml GM-CSF (R&D systems) for 6 days. 5×10^5 cells were seeded into a 24 well plate and infected with MNV CR6 (MOI 1) for 1h at 37°C. Virus was removed and BMDCs cultured for a further 16h before harvesting RNA. Murine SI organoids were grown for 3–5 days before gentle disruption and re-culturing of approximately 200 organoids/well in the presence of 3×10^6 pfu of MNV CR6 for 16 h.

Microscopy on intestinal tissue

Small intestinal and colonic tissue was prepared for staining as previously described³. Hematoxylin and eosin (H&E) staining was performed by the NYU Histopathology core. Ki67, phospho-Stat1 and phospho-Stat3 staining were performed by NYU Immunohistochemistry (IHC) core. Formalin fixed paraffin-embedded sections were deparaffinized and antigen retrieved in Ventana Cell Conditioner 2 (Citrate). Endogenous peroxidase activity was blocked with hydrogen peroxide and tissue was incubated with unconjugated rabbit anti-mouse phospho-Stat1 (Tyr701, Cell Signaling Technology), rabbit

anti-mouse phospho-Stat3 (Tyr705, Cell Signaling Technology) or rabbit anti-mouse Ki67 (M3062) (Spring Biosciences). Signal was detected with anti-rabbit horseradish peroxidase conjugated multimer and visualized with 3,3 diaminobenzidine. At least 50 small intestinal villi per mouse were measured for villi width at the base of the villi. At least 50 colon crypts were analyzed for the number of Ki67⁺ cells. At least 20 sections along the length of the colon were scored for pSTAT expression. The scoring criteria for pSTAT staining was as follows: 0 = no staining; 1 = 1 or 2 individual positive cells; 2 = 10% positive cells; 3 = 10–30% positive cells; 4 = 30–75% positive cells and 5 = >75% positive cells. Severity of colon pathology was blindly quantified by a pathologist (A.G.N). Mice received a pathology score between 0 and 4 for inflammatory cell infiltration, inflammatory cell location and depth, edema and necrosis. A score of 0 = negative pathology, 1 = minimal, 2 = mild, 3 = moderate and 4 = marked pathology for the indicated fields. Crypt hyperplasia was scored by measuring crypt length and given an average score as follows: 0 = <100µM, 1 = 100–150µM, 2 = 150–200µM, 3 = 200–250µM and 4 = >250µM. Mean values were calculated for each mouse and used as individual data points. Sections were imaged either on an Axioplan microscope (Zeiss) or Evos FL Auto (Thermo Fisher Scientific). All analyses were performed using ImageJ software.

Microscopy on intestinal organoids

Organoids were frozen in Neg 50 frozen section medium (Thermo Fisher Scientific) and sectioned at 5µm. Tissue was permeabilized with 0.1% (v/v) Tween 20 (Sigma Aldrich) and 0.01% (v/v) TritonX (Sigma Aldrich) followed by blocking with 1% (w/v) BSA (Fisher Scientific). Staining was performed using sheep anti-mouse Reg3β antibody (R&D systems) followed by detection with anti-sheep Ig NL557 (R&D systems) and mounting with Vectashield containing Dapi (Vector Laboratories). Sections were imaged on the Evos FL Auto (Thermo Fisher Scientific). All analyses were performed using ImageJ software. Mean fluorescence intensity values were calculated for each organoid and used as individual data points.

Flow cytometry

Lamina propria cells from colonic tissue were harvested as before⁸. For intracellular cytokine staining, cells were stimulated using the eBioscience cell stimulation cocktail for 4 h at 37 °C. Cells were fixed and permeabilized using the Biolegend fixation and permeabilization buffer. The following antibodies (clones) were used for staining: CD45 (30-F11), CD19 (6D5), CD11b (M1/70), CD90.2 (53–2.1), CD3 (145–2C11), TCR-β (H57–597), CD4 (RM4–5), CD8 (53–6.7), Gr-1 (RB6–8C5), MHCII (M5/114.15.2), CD11c (N418), CD103 (2E7), IFN-γ (XMG1.2) from Biolegend and IL-22 (1H8PWSR), and IL-13 (eBio13A) from eBioscience. All samples were blocked with Fc block (TruStainfcx) and stained with a fixable live dead stain (Invitrogen). FlowJo v.10 was used to analyze flow cytometry data. Intestinal epithelial cells (IECs) were harvested by incubation at 37°C with 2mM DTT (Sigma) followed by two incubations with 5mM EDTA and then digested with Dispase (Sigma) and DNase (Sigma). IECs were sorted as PI⁻CD45⁻EpCam⁺ using the following antibody clones: CD45 (30-F11) and EpCam (G8.8) from Biolegend on a FACSAria II (BD Biosciences). Purity of IECs was 95%.

Colon explant culture and IL-22 detection

1cm of colon tissue was opened longitudinally, washed with PBS and cultured for 48 h in 500 μ l of complete RPMI containing 2 mM L-glutamine (Corning), penicillin/streptomycin solution (Corning), 20 mM HEPES (Corning), MEM non-essential amino acids (Corning), 1 mM Sodium pyruvate (Corning) and β -mercaptoethanol (Gibco). IL-22 in supernatants was measured using the mouse IL-22 ELISA MAX Deluxe kit (Biolegend) according to the manufacturer's instructions.

RNA isolation and qPCR

RNA from BMDCs and colonic tissue (1 cm) homogenized using a TissueRuptor (Qiagen) was isolated using the Qiagen RNeasy mini kit with DNase treatment (Qiagen). RNA from sorted IECs and LPLs was isolated using the RNeasy Micro Kit with DNase treatment (Qiagen). RNA from intestinal organoids was isolated with TRIzol reagent (Fisher Scientific) using the manufacturer's protocol and DNA digested using RNase-free DNase (Thermo Fisher Scientific). cDNA synthesis was conducted with the ProtoScript M-MuLV First Strand cDNA synthesis kit (New England Biolabs). qPCR was performed using SybrGreen (Roche) on a Roche480II Lightcycler using the following primers: *mHprt* (Accession no. J00423), Fwd 5'-GTCATGCCGACCCGACAGTC-3', Rev 5'-GTCCTGTCCATAATCAGTCCATGAGGAATAAAC-3'; *m18S* (Accession no. NR_003278), Fwd 5'-TAGAGGGACAAGTGGCGTTC-3', Rev 5'-CGCTGAGCCAGTCAGTGT-3'; *mIfnb1* (Accession no. X14455), Fwd 5'-TCAGAATGAGTGGTGGTTGC-3', Rev 5'-GACCTTTCAAATCGAGTAGATTCA-3'; *mMx2* (Accession no. KX774217), Fwd 5'-CCAGTTCCTCTCAGTCCCAAGATT-3', Rev 5'-TACTGGATGATCAAGGGAACGTGG-3'; *mOasL2* (Accession no. NM_011854), Fwd 5'-GGATGCCTGGGAGAGAATCG-3', Rev 5'-TCGCCTGCTCTTCGAAACTG-3'; *mIsg15* (Accession no. NM_015783), Fwd 5'-GGTGTCCGTGACTAACTCCAT-3', Rev 5'-TGGAAGGGTAAGACCGTCCT-3'; *h β -actin* (Accession no. NM_001101), Fwd 5'-TCACCGGAGTCCATCACGAT-3', Rev 5'-CCCAGCCATGTACGTTGCTA-3' and *hMx2* (Accession no. NM_002463), Fwd 5'-AAACTGTTTCAGAGCACGATTGAAG-3', Rev 5'-ACCATCTGCTCCATTCTGAACTG-3'. Relative expression of the respective genes to either *Hprt* (murine organoids), *18S* (murine colon or sorted cells) or β -actin (human organoids) expression was calculated using the C_T method and values were expressed as fold change from uninfected mice or untreated organoids. Absolute MNV genome copies were determined using a standard curve and the following primers: Fwd 5'-CAGATCACATGCTTCCCAC-3' and Rev 5'-AGACCACAAAAGACTCATCAC-3'.

Immunoblotting

Organoids were isolated and processed for immunoblotting as previously described⁷. Briefly, protein was run through a 4–12% gradient protein gel (BioRad), transferred onto a PVDF membrane and blocked using Odyssey Blocking buffer (LI-COR). Membranes were stained with mouse anti-STAT3 and rabbit anti-pSTAT3 (Tyr705) and detected using IRDye 680RD goat anti-rabbit IgG and IRDye 800CW goat anti-mouse IgG (LI-COR) on an Odyssey CLx near-infrared fluorescence imaging system.

RNA deep sequencing

cDNA libraries were prepared with the Ovation Trio Low Input RNA-seq System V2 (NuGEN) and sequenced on Illumina's HiSeq platform using a paired-end protocol at the NYU Genomics Core. On average, each sample yielded 25 million paired reads, which passed FASTQC quality control. Sequencing reads were aligned with STAR v2.6.1d against the GRCm38.p6 genome assembly, resulting in an average of 20 million aligned pairs per sample, and normalized read counts were calculated using Cufflinks v2.2.1 against the same reference genome. Differential gene expression was determined with Cuffdiff and gene ontology analysis performed using Qiagen's Ingenuity Pathway Analysis (IPA, Qiagen).

16S library preparation and sequencing analysis

DNA was isolated from stool samples using the NucleospinSoil Kit (Macherey-Nagel). Bacterial 16S rRNA gene was amplified at the V4 region using primer pairs and paired-end amplicon sequencing was performed on the Illumina MiSeq system. Sequencing reads were processed using the DADA2 pipeline in the QIIME2 software package⁴⁷. Beta diversity was calculated using unweighted UniFrac distance^{48,49}. Principle Coordinate Analysis (PCoA) was performed on the UniFrac distance matrix and visualized with EMPeror⁵⁰.

Statistical Analysis

All data was analyzed using Graphpad Prism v.7. All graphs show the mean and standard error of the mean (SEM). The number of samples per group is indicated in the figure legend. The log-rank Mantel-Cox test was used for comparison of survival curves. An unpaired two-tailed *t*-test was used to evaluate differences between two groups. Welch's correction was used when variances were significantly different between groups. An analysis of variance (ANOVA) with Dunnett's or Tukey's multiple comparisons test was used to evaluate experiments involving multiple groups. For bacterial and viral titers, log₁₀ transformed data was analyzed. Correlation was analyzed using Pearson *r*. Weight curves were analyzed using area under the curve (AUC) followed by two-tailed *t*-test. All *p*-values are shown in figures.

Supplementary Material

Refer to Web version on PubMed Central for supplementary material.

Acknowledgements

We wish to thank the following NYU facilities for use of their instruments and technical assistance: Microcopy Core (RR023704), Histopathology and Immunohistochemistry Core (P30CA016087, NIH S10 OD010584-01A1, and S10 OD018338-01), the Cytometry and Cell Sorting Laboratory (P30CA016087), the Genome Technology Center (P30CA016087), and the Gnotobiotic Facility (Colton Center for Autoimmunity). We also wish to thank Satoru Fujii (Washington University School of Medicine in St. Louis) for his technical support in human organoid culture. This research was supported by US National Institute of Health (NIH) grants R01 HL123340 (K.C.), R01 DK093668 (K.C.), R01 DK103788 (K.C. and P.L.), R01 AI121244 (K.C.), and R01 AI130945 (P.L.). This work was also supported by Vilcek Fellowship (J.A.N.), Sir Keith Murdoch Fellowship (J.A.N.), Crohn's & Colitis Foundation Research Fellowship Award (Y.M-I); Faculty Scholar grant from the Howard Hughes Medical Institute (K.C.), Advanced Research Grant from the Merieux Institute (K.C.), Rainin Foundation Innovator Award (K.C.), Stony Wold-Herbert Fund (K.C.), PureTech Health (K.C.), Pfizer (K.C. and P.L.), NYU CTSI (NIH/NCATS 1UL TR001445; K.C. and P.L.), and philanthropy from Bernard Levine (K.C. and P.L.); and K.C. is a Burroughs Wellcome Fund Investigator in the Pathogenesis of Infectious Diseases.

References

1. Cadwell K The virome in host health and disease. *Immunity* 42, 805–813 (2015). [PubMed: 25992857]
2. Neil JA & Cadwell K The Intestinal Virome and Immunity. *J Immunol* 201, 1615–1624 (2018). [PubMed: 30181300]
3. Cadwell K, et al. Virus-plus-susceptibility gene interaction determines Crohn’s disease gene Atg16L1 phenotypes in intestine. *Cell* 141, 1135–1145 (2010). [PubMed: 20602997]
4. Basic M, et al. Norovirus triggered microbiota-driven mucosal inflammation in interleukin 10-deficient mice. *Inflamm Bowel Dis* 20, 431–443 (2014). [PubMed: 24487272]
5. Seamons A, et al. Obstructive Lymphangitis Precedes Colitis in Murine Norovirus-Infected Stat1-Deficient Mice. *Am J Pathol* (2018).
6. Cadwell K, et al. A key role for autophagy and the autophagy gene Atg16l1 in mouse and human intestinal Paneth cells. *Nature* 456, 259–263 (2008). [PubMed: 18849966]
7. Matsuzawa-Ishimoto Y, et al. Autophagy protein ATG16L1 prevents necroptosis in the intestinal epithelium. *J Exp Med* 214, 3687–3705 (2017). [PubMed: 29089374]
8. Kernbauer E, Ding Y & Cadwell K An enteric virus can replace the beneficial function of commensal bacteria. *Nature* 516, 94–98 (2014). [PubMed: 25409145]
9. Abt MC, et al. TLR-7 activation enhances IL-22-mediated colonization resistance against vancomycin-resistant enterococcus. *Sci Transl Med* 8, 327ra325 (2016).
10. Thepaut M, et al. Protective role of murine norovirus against *Pseudomonas aeruginosa* acute pneumonia. *Vet Res* 46, 91 (2015). [PubMed: 26338794]
11. Yang JY, et al. Enteric Viruses Ameliorate Gut Inflammation via Toll-like Receptor 3 and Toll-like Receptor 7-Mediated Interferon-beta Production. *Immunity* 44, 889–900 (2016). [PubMed: 27084119]
12. Vijay-Kumar M, et al. Activation of toll-like receptor 3 protects against DSS-induced acute colitis. *Inflamm Bowel Dis* 13, 856–864 (2007). [PubMed: 17393379]
13. Bailey D, Thackray LB & Goodfellow IG A single amino acid substitution in the murine norovirus capsid protein is sufficient for attenuation in vivo. *J Virol* 82, 7725–7728 (2008). [PubMed: 18495770]
14. Strong DW, Thackray LB, Smith TJ & Virgin HW Protruding domain of capsid protein is necessary and sufficient to determine murine norovirus replication and pathogenesis in vivo. *J Virol* 86, 2950–2958 (2012). [PubMed: 22258242]
15. Zhu S, et al. Regulation of Norovirus Virulence by the VP1 Protruding Domain Correlates with B Cell Infection Efficiency. *J Virol* 90, 2858–2867 (2015). [PubMed: 26719276]
16. Tomov VT, et al. Persistent enteric murine norovirus infection is associated with functionally suboptimal virus-specific CD8 T cell responses. *J Virol* 87, 7015–7031 (2013). [PubMed: 23596300]
17. Nice TJ, Strong DW, McCune BT, Pohl CS & Virgin HW A single-amino-acid change in murine norovirus NS1/2 is sufficient for colonic tropism and persistence. *J Virol* 87, 327–334 (2013). [PubMed: 23077309]
18. Jones MK, et al. Enteric bacteria promote human and mouse norovirus infection of B cells. *Science* 346, 755–759 (2014). [PubMed: 25378626]
19. Baldridge MT, et al. Commensal microbes and interferon-lambda determine persistence of enteric murine norovirus infection. *Science* 347, 266–269 (2015). [PubMed: 25431490]
20. Lee S, et al. Norovirus Cell Tropism Is Determined by Combinatorial Action of a Viral Non-structural Protein and Host Cytokine. *Cell Host Microbe* 22, 449–459 e444 (2017). [PubMed: 28966054]
21. Wilen CB, et al. Tropism for tuft cells determines immune promotion of norovirus pathogenesis. *Science* 360, 204–208 (2018). [PubMed: 29650672]
22. Sun L, et al. Type I interferons link viral infection to enhanced epithelial turnover and repair. *Cell Host Microbe* 17, 85–97 (2015). [PubMed: 25482432]

23. McCartney SA, et al. MDA-5 recognition of a murine norovirus. *PLoS Pathog* 4, e1000108 (2008). [PubMed: 18636103]
24. Wang P, et al. Nlrp6 regulates intestinal antiviral innate immunity. *Science* 350, 826–830 (2015). [PubMed: 26494172]
25. MacDuff DA, et al. HOIL1 Is Essential for the Induction of Type I and III Interferons by MDA5 and Regulates Persistent Murine Norovirus Infection. *J Virol* 92(2018).
26. Pickert G, et al. STAT3 links IL-22 signaling in intestinal epithelial cells to mucosal wound healing. *J Exp Med* 206, 1465–1472 (2009). [PubMed: 19564350]
27. Seo SU, et al. Intestinal macrophages arising from CCR2(+) monocytes control pathogen infection by activating innate lymphoid cells. *Nat Commun* 6, 8010 (2015). [PubMed: 26269452]
28. Tschurtschenthaler M, et al. Type I interferon signalling in the intestinal epithelium affects Paneth cells, microbial ecology and epithelial regeneration. *Gut* 63, 1921–1931 (2014). [PubMed: 24555997]
29. Pott J, et al. IFN-lambda determines the intestinal epithelial antiviral host defense. *Proc Natl Acad Sci U S A* 108, 7944–7949 (2011). [PubMed: 21518880]
30. Baldrige MT, et al. Expression of Ifnlr1 on Intestinal Epithelial Cells Is Critical to the Antiviral Effects of Interferon Lambda against Norovirus and Reovirus. *J Virol* 91, pii: e02079–02016 (2017). [PubMed: 28077655]
31. Nice TJ, et al. Interferon-lambda cures persistent murine norovirus infection in the absence of adaptive immunity. *Science* 347, 269–273 (2015). [PubMed: 25431489]
32. Gronke K, et al. Interleukin-22 protects intestinal stem cells against genotoxic stress. *Nature* 566, 249–253 (2019). [PubMed: 30700914]
33. Lim ES, et al. Early life dynamics of the human gut virome and bacterial microbiome in infants. *Nat Med* 21, 1228–1234 (2015). [PubMed: 26366711]
34. Mao K, et al. Innate and adaptive lymphocytes sequentially shape the gut microbiota and lipid metabolism. *Nature* 554, 255–259 (2018). [PubMed: 29364878]
35. Zheng Y, et al. Interleukin-22 mediates early host defense against attaching and effacing bacterial pathogens. *Nat Med* 14, 282–289 (2008). [PubMed: 18264109]
36. Kim YG, et al. Neonatal acquisition of Clostridia species protects against colonization by bacterial pathogens. *Science* 356, 315–319 (2017). [PubMed: 28428425]
37. Ettayebi K & Hardy ME Norwalk virus nonstructural protein p48 forms a complex with the SNARE regulator VAP-A and prevents cell surface expression of vesicular stomatitis virus G protein. *J Virol* 77, 11790–11797 (2003). [PubMed: 14557663]
38. Fernandez-Vega V, et al. Norwalk virus N-terminal nonstructural protein is associated with disassembly of the Golgi complex in transfected cells. *J Virol* 78, 4827–4837 (2004). [PubMed: 15078964]
39. McCune BT, et al. Noroviruses Co-opt the Function of Host Proteins VAPA and VAPB for Replication via a Phenylalanine-Phenylalanine-Acidic-Tract-Motif Mimic in Nonstructural Viral Protein NS1/2. *MBio* 8(2017).
40. Baker ES, et al. Inherent structural disorder and dimerisation of murine norovirus NS1–2 protein. *PLoS One* 7, e30534 (2012). [PubMed: 22347381]
41. Broggi A, Tan Y, Granucci F & Zanoni I IFN-lambda suppresses intestinal inflammation by non-translational regulation of neutrophil function. *Nat Immunol* 18, 1084–1093 (2017). [PubMed: 28846084]
42. Martin PK, et al. Autophagy proteins suppress protective type I interferon signalling in response to the murine gut microbiota. *Nat Microbiol* 3, 1131–1141 (2018). [PubMed: 30202015]
43. Van Winkle JA, et al. Persistence of Systemic Murine Norovirus Is Maintained by Inflammatory Recruitment of Susceptible Myeloid Cells. *Cell Host Microbe* 24, 665–676 e664 (2018). [PubMed: 30392829]
44. Phillips G, Tam CC, Rodrigues LC & Lopman B Prevalence and characteristics of asymptomatic norovirus infection in the community in England. *Epidemiol Infect* 138, 1454–1458 (2010). [PubMed: 20196905]

45. Bouziat R, et al. Reovirus infection triggers inflammatory responses to dietary antigens and development of celiac disease. *Science* 356, 44–50 (2017). [PubMed: 28386004]
46. Bouziat R, et al. Murine Norovirus Infection Induces TH1 Inflammatory Responses to Dietary Antigens. *Cell Host Microbe* 24, 677–688 e675 (2018). [PubMed: 30392830]
47. Caporaso JG, et al. QIIME allows analysis of high-throughput community sequencing data. *Nat Methods* 7, 335–336 (2010). [PubMed: 20383131]
48. Chen J, et al. Associating microbiome composition with environmental covariates using generalized UniFrac distances. *Bioinformatics* 28, 2106–2113 (2012). [PubMed: 22711789]
49. Lozupone C, Lladser ME, Knights D, Stombaugh J & Knight R UniFrac: an effective distance metric for microbial community comparison. *ISME J* 5, 169–172 (2011). [PubMed: 20827291]
50. Vazquez-Baeza Y, Pirrung M, Gonzalez A & Knight R EMPeror: a tool for visualizing high-throughput microbial community data. *Gigascience* 2, 16 (2013). [PubMed: 24280061]

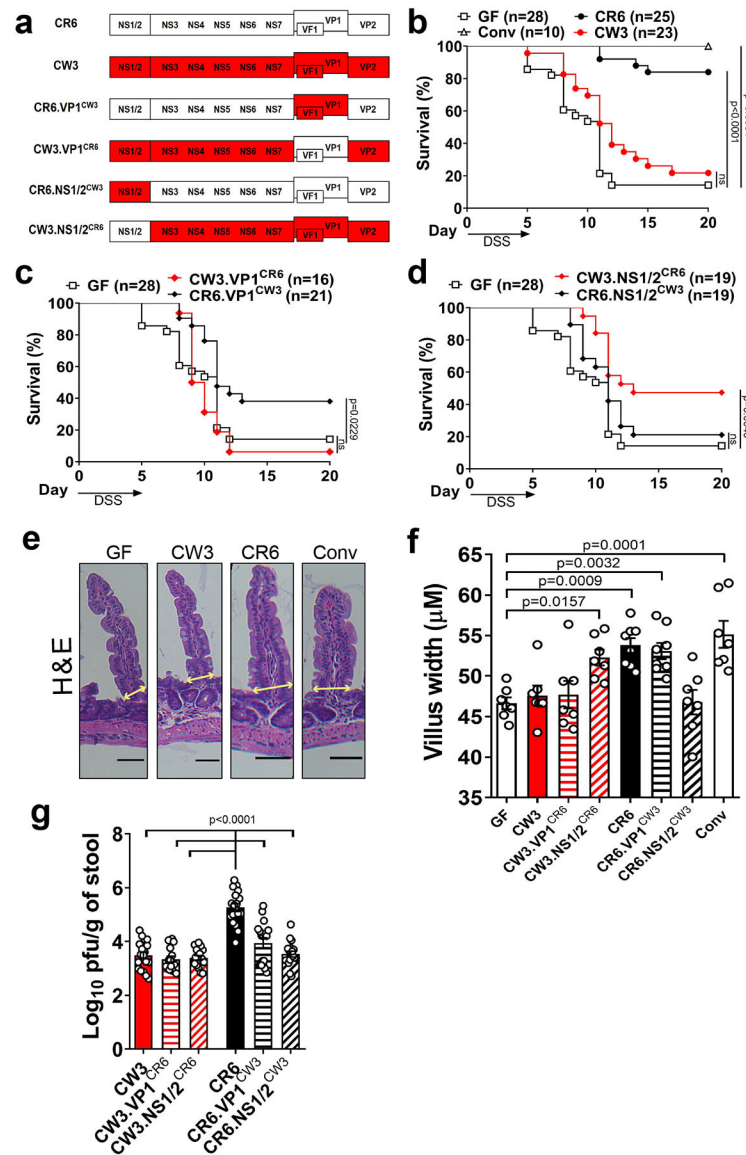


Figure 1: Sequence variation in NS1/2 contributes to protection from intestinal injury.

(a) Illustration of parental and chimeric MNV strains. (b) Survival of uninfected GF, MNV-infected GF mice (CR6 and CW3) and conventional (Conv) mice following administration of 3% DSS in the drinking water for 5 days. Survival of GF mice infected with VP1 (c) or NS1/2 (d) chimeric viruses following DSS. Mice were infected for 10 days prior to DSS administration. Survival experiments with the parental strains and chimeric viruses were conducted concurrently and therefore the uninfected GF survival curve shown in (b), (c) and (d) are identical. Representative H&E images of small intestinal villi (e) and quantification of villus width (f) at 10 dpi. Scale bars represent 50μM. All groups have 7 mice except for CR6 and CR6.VP1^{CW3} that have 8 mice. (g) Infectious MNV in the stool as determined by plaque assay at 10 dpi. The following mice were analyzed per group: CW3, n=18; CW3.VP1^{CR6}, n=15; CW3.NS1/2^{CR6}, n=17; CR6, n=18; CR6.VP1^{CW3}, n=17 and CR6.NS1/2^{CW3}, n=18. Survival curves were analyzed using the log-rank Mantel–Cox test.

Villus width and \log_{10} transformed stool titers were analyzed using ANOVA with Dunnett's multiple comparisons test compared to GF mice or CR6-infected GF mice, respectively. All bars represent mean and error bars represent standard error of the mean. All p-values are shown in the figure.

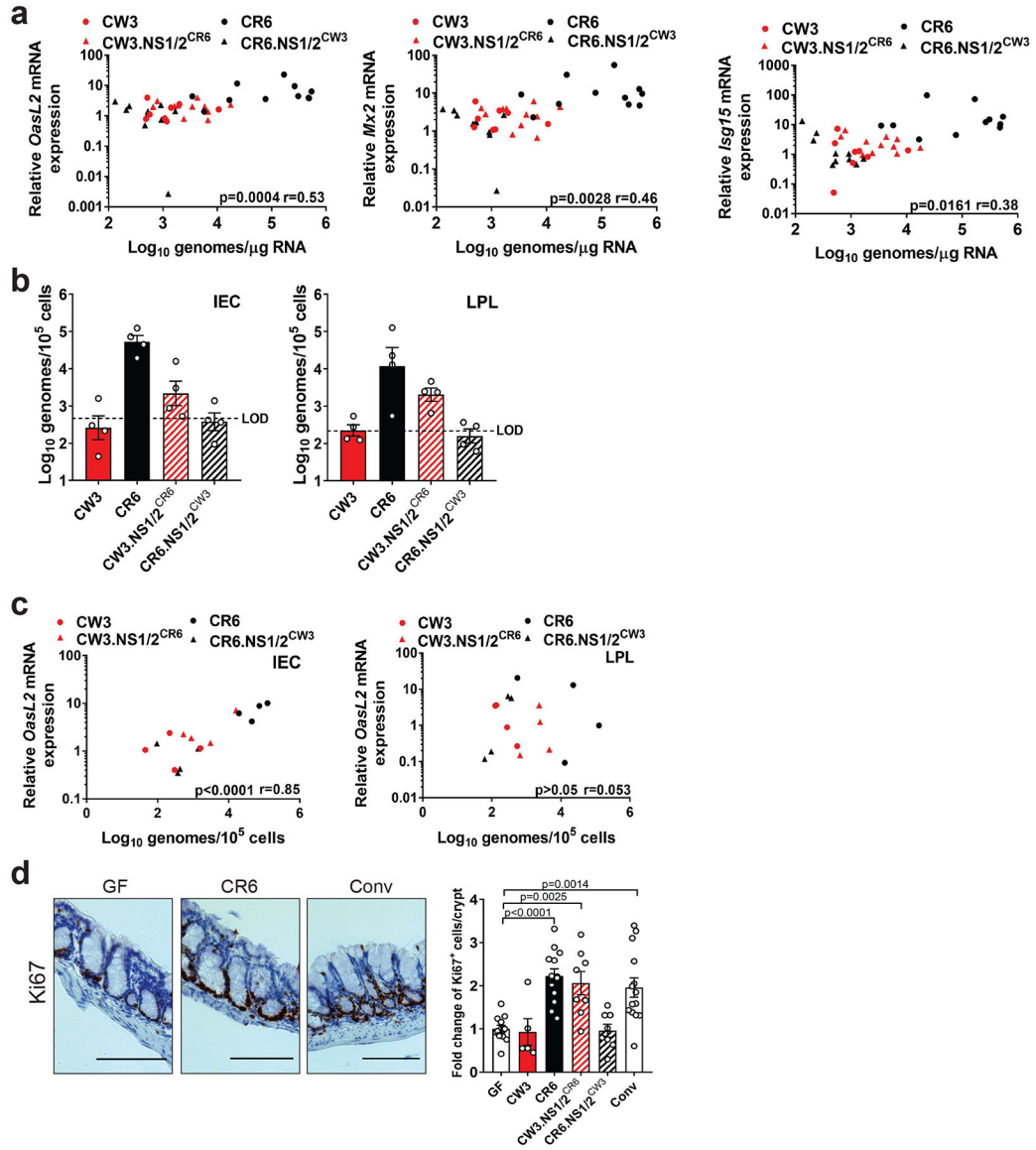


Figure 2: NS1/2 sequence variation contributes to intestinal persistence, IFN-I signaling and epithelial cell proliferation following intestinal injury.

(a) *OasL2*, *Mx2* and *Isg15* mRNA expression over uninfected GF mice relative to viral \log_{10} genomes in the colon. Data represents 4 independent experiments. The following mice were analyzed per group: CW3, n=8; CR6, n=11; CW3.NS1/2^{CR6}, n=11 and CR6.NS1/2^{CW3}, n=10. (b) Viral genomes in sorted colonic IECs and LPLs. LOD=limit of detection. Data represents 2 independent experiments each with 2 mice per group. (c) *OasL2* mRNA expression over uninfected GF mice relative to viral \log_{10} genomes in IECs and LPLs. Data represents 2 independent experiments each with 2 mice per group. (d) Representative images of the colon stained for Ki67 and corresponding fold change of Ki67⁺ IECs relative to uninfected GF mice. Scale bars represent 100 μM . The following mice were analyzed per group: GF, n=12; CW3, n=5; CR6, n=13; CW3.NS1/2^{CR6}, n=8; CR6.NS1/2^{CW3}, n=8 and Conv, n=14. All samples were analyzed at day 5 of DSS administration. Correlation was analyzed using Pearson r with p-values and r-values as shown. Fold change of Ki67⁺ IEC/

crypt was analyzed using ANOVA with Dunnett's multiple comparisons test with p-values shown. All bars represent mean and error bars represent standard error of the mean.

Author Manuscript

Author Manuscript

Author Manuscript

Author Manuscript

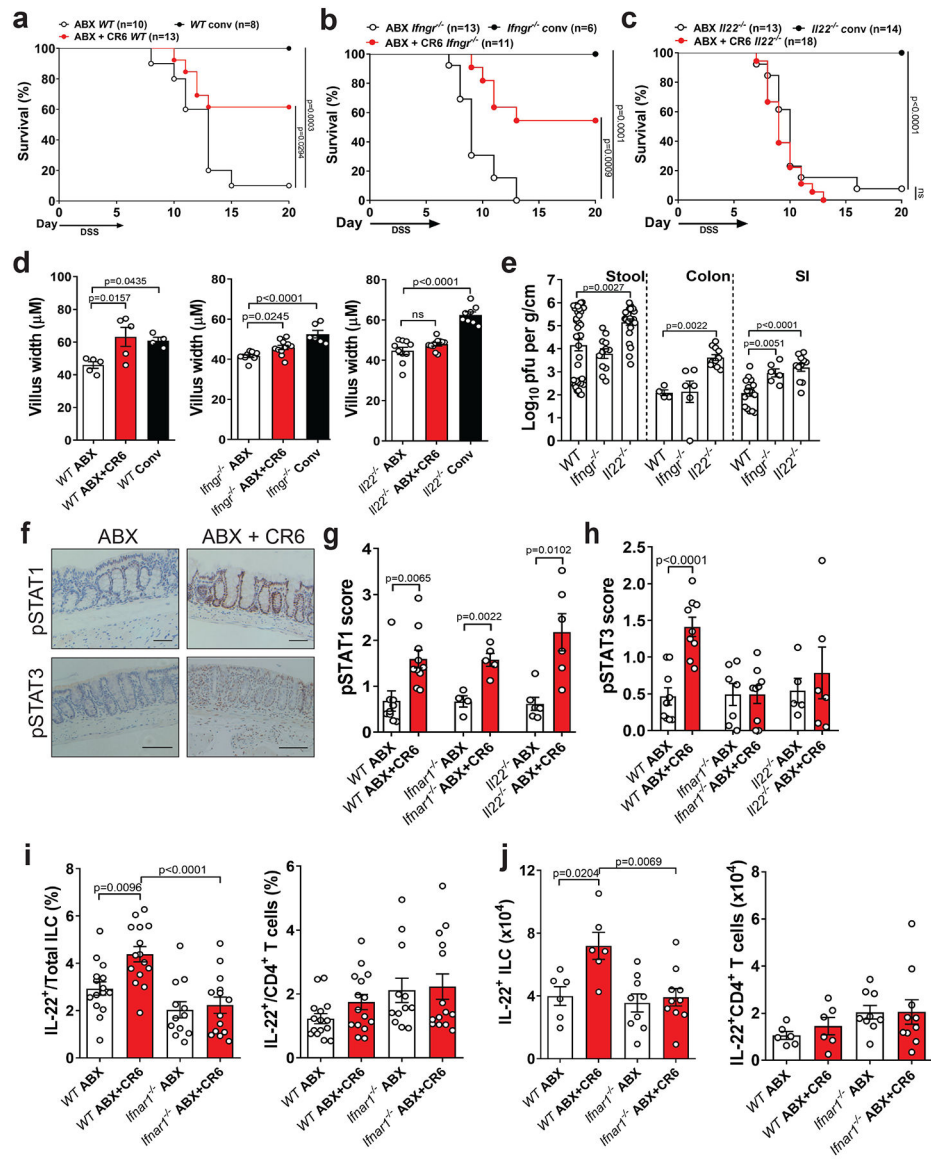


Figure 3: Protection of ABX-treated mice from intestinal injury is dependent on IL-22. Survival of *WT* (a), *Ifnar1*^{-/-} (b) and *Il22*^{-/-} (c) mice following DSS. Mice were treated with ABX for at least 10 days prior to CR6 infection and given DSS at 10 dpi for 6 days. Small intestinal villus width (d) and virus levels in the stool, colon and SI (e) at 10 dpi with CR6. The following ABX, ABX+CR6 and Conv mice were analyzed for villus width: *WT* n=5,5,4; *Ifnar1*^{-/-}, n=9,11,6 and *Il22*^{-/-}, n=10,11,8. The following mice were analyzed for stool, colon and SI titer: *WT*, n=36,4,17; *Ifnar1*^{-/-}, n=12,6,6 and *Il22*^{-/-}, n=25,11,11. (f) Representative images of pSTAT1 and pSTAT3 expression in the colon of ABX-treated *WT* mice. Scale bars represent 100μm. pSTAT1 (g) and pSTAT3 (h) expression score in the colon at day 6 post DSS. The following mice were analyzed for pSTAT1 and pSTAT3: *WT* ABX, n=9,9; *WT* ABX+CR6, n=10,9; *Ifnar1*^{-/-} ABX, n=4,8; *Ifnar1*^{-/-} ABX+CR6, n=5,9; *Il22*^{-/-} ABX, n=6,5 and *Il22*^{-/-} ABX+CR6, n=6,6. Proportion (i) and absolute numbers (j) of IL-22 expressing ILC (CD19⁻CD11b⁻CD90.2⁺CD3⁻TCRβ⁻) and CD4⁺ T cells

(CD19⁻CD11b⁻CD90.2⁺CD3⁺TCR β ⁺CD4⁺) in the colon of ABX-treated *WT* and *Ifnar1*^{-/-} mice at day 6 post DSS. The following mice were analyzed for cell proportions and numbers: *WT* ABX, n=15,6; *WT* ABX+CR6, n=15,6; *Ifnar1*^{-/-} ABX, n=12,9 and *Ifnar1*^{-/-} ABX+CR6, n=14,10. Survival curves were analyzed using the log-rank Mantel–Cox test. ANOVA with Dunnett’s multiple comparisons test was used to analyze villus width and Log₁₀ transformed MNV titer compared to ABX and *WT* mice, respectively. A two-tailed t-test was used to analyze STAT expression. ANOVA with Tukey’s multiple comparisons test was used to analyze flow cytometry data. All bars represent mean and error bars represent standard error of the mean. All p-values are shown in the figure.

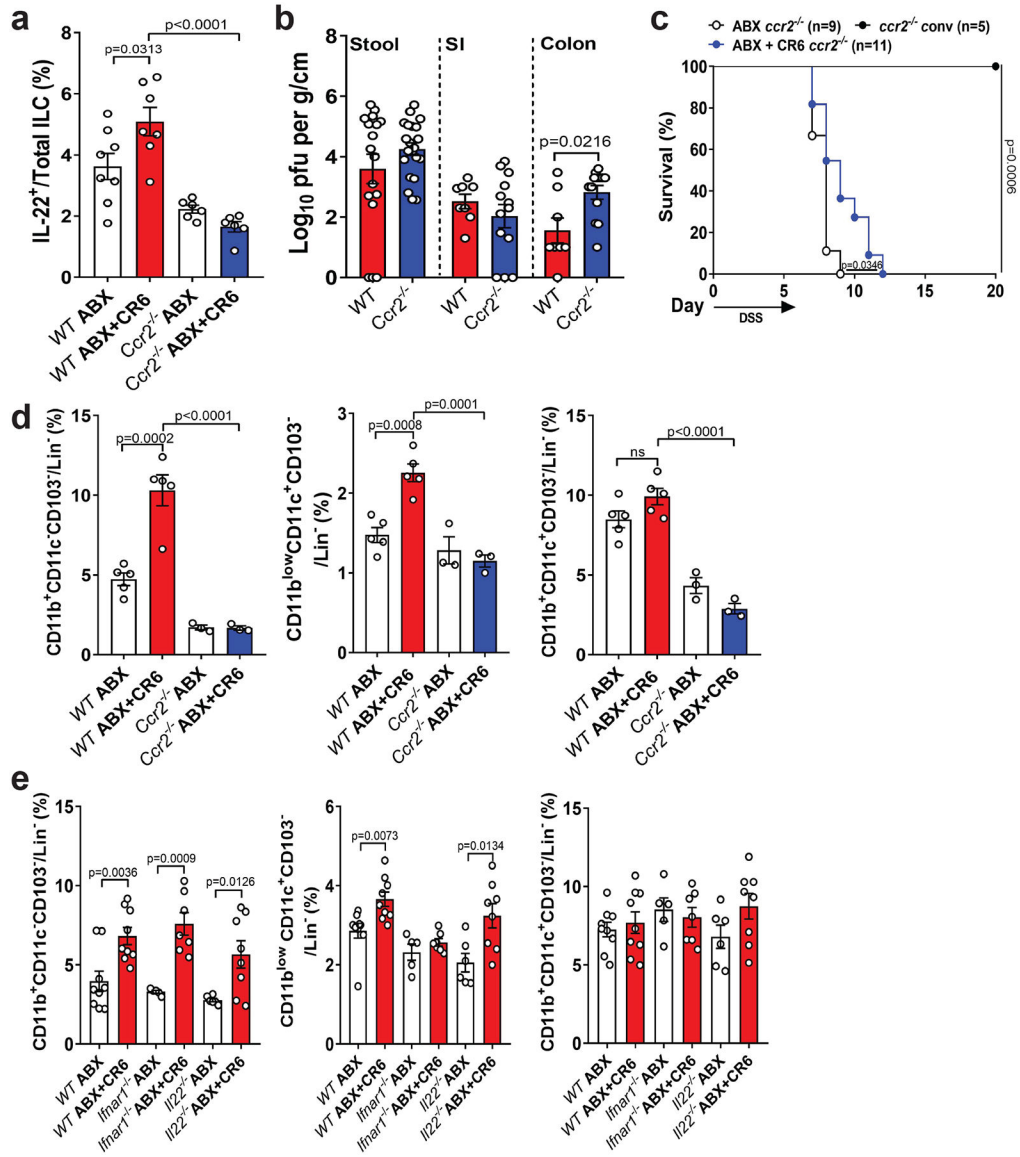


Figure 4: Protection from intestinal injury and IL-22 expression is associated with CCR2-dependent cells.

(a) Proportion of IL-22 expressing ILC in ABX-treated *WT* and *CCR2*^{-/-} mice at day 6 post DSS. The following number of mice were analyzed: *WT* ABX, n=8; *WT* ABX+CR6, n=7; *CCR2*^{-/-} ABX, n=6 and *CCR2*^{-/-} ABX+CR6, n=6. (b) Infectious virus levels in the SI, colon and stool of ABX-treated *CCR2*^{-/-} mice compared to *WT* mice. The following number of mice were analyzed for stool titer: *WT*, n=17 and *CCR2*^{-/-}, n=22; SI and colon titer: *WT*, n=8 and *CCR2*^{-/-}, n=13. (c) Survival of *CCR2*^{-/-} mice following DSS administration. Mice were treated with ABX for at least 10 days prior to CR6 infection and given DSS at 10 dpi for 6 days. Survival curves were analyzed using the log-rank Mantel–Cox test. Proportion of MHCII⁺ populations in ABX-treated *WT* and *CCR2*^{-/-} (d) and ABX-treated *WT*, *Ifnar1*^{-/-} and *Il22*^{-/-} (e) mice at day 6 post DSS. The following number of mice were analyzed in (d): *WT* ABX, n=5; *WT* ABX+CR6, n=5; *CCR2*^{-/-} ABX, n=3 and *CCR2*^{-/-} ABX+CR6, n=3. The following number of mice were analyzed in (e): *WT* ABX, n=9; *WT* ABX+CR6, n=9;

Ifnar1^{-/-} ABX, n=5; *Ifnar1*^{-/-} ABX+CR6, n=7; *Il22*^{-/-} ABX, n=6 and *Il22*^{-/-} ABX+CR6, n=8. Lin⁻ = CD45⁺CD19⁻TCRβ⁻Gr-1^{low}. Figures (a) and (d) were analyzed using ANOVA with Tukey's multiple comparisons test and figure (b) and (e) were analyzed using two-tailed t-test. All bars represent mean and error bars represent standard error of the mean. All p-values are shown in the figure.

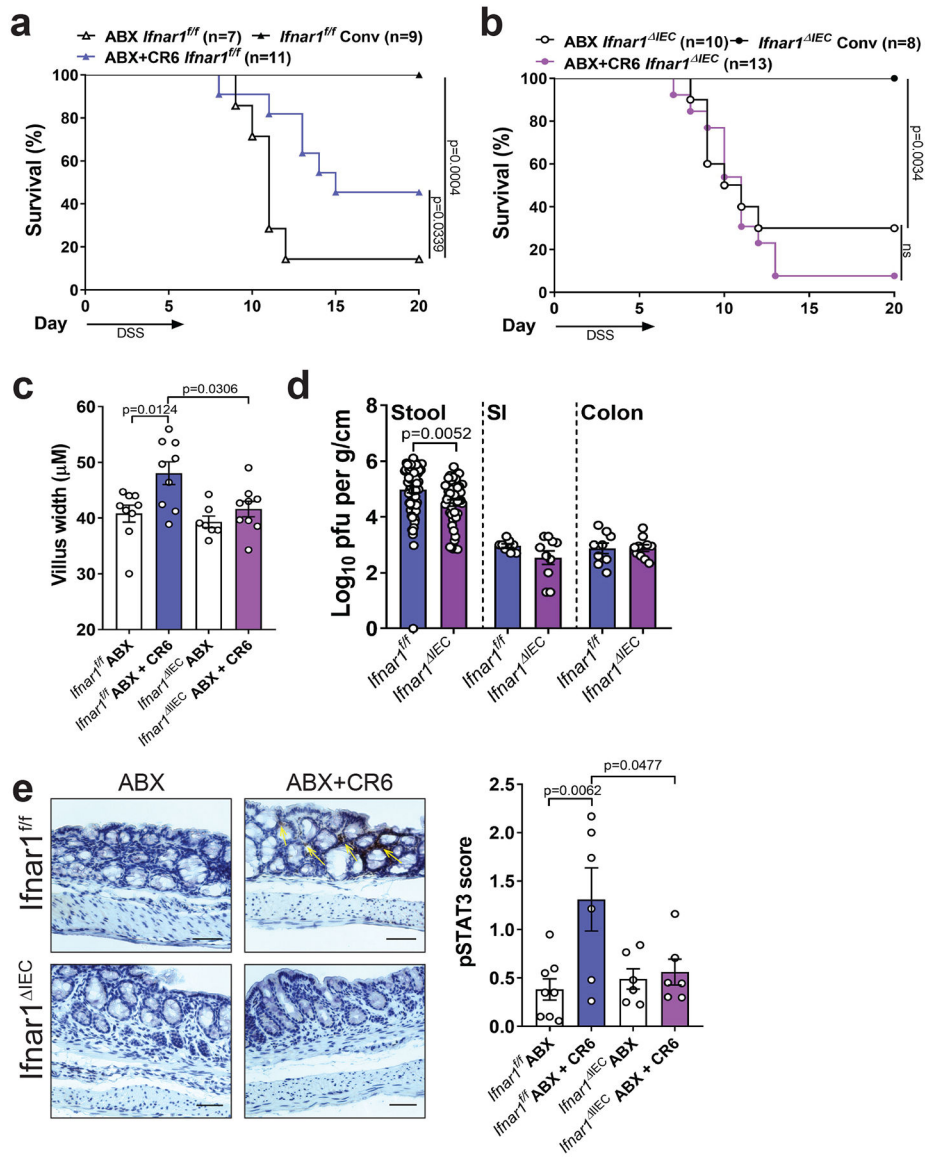


Figure 5: IFN-I signaling in IEC is required for protection from intestinal injury. Survival of *Ifnar1^{fl/fl}* (a) and *Ifnar1^{IEC}* (b) mice following DSS. Mice were treated with ABX for at least 10 days prior to CR6 infection and given DSS at 10 dpi for 6 days. Survival curves were analyzed using the log-rank Mantel–Cox test. Small intestinal villus width (c) and virus levels in the SI, colon and stool (d) at 10 dpi with CR6. The following number of mice were analyzed for villus width: *Ifnar1^{fl/fl}* ABX, n=9; *Ifnar1^{fl/fl}* ABX+CR6, n=9; *Ifnar1^{IEC}* ABX, n=7 and *Ifnar1^{IEC}* ABX+CR6, n=9. The following number of mice were analyzed for stool titer: *Ifnar1^{fl/fl}*, n=71 and *Ifnar1^{IEC}*, n=49; SI and colon titer: *Ifnar1^{fl/fl}*, n=9 and *Ifnar1^{IEC}*, n=10. (e) Representative images of pSTAT3 staining in the colon and pSTAT3 expression score at day 6 post DSS. Scale bars represent 100μM. The following number of mice were analyzed for pSTAT3: *Ifnar1^{fl/fl}* ABX, n=8; *Ifnar1^{fl/fl}* ABX+CR6, n=6; *Ifnar1^{IEC}* ABX, n=6 and *Ifnar1^{IEC}* ABX+CR6, n=6. Figures (c) and (e) were analyzed using ANOVA with Tukey’s multiple comparisons test and figure (d) was analyzed using

two-tailed t-test. All bars represent mean and error bars represent standard error of the mean. All p-values are shown in the figure.

Author Manuscript

Author Manuscript

Author Manuscript

Author Manuscript

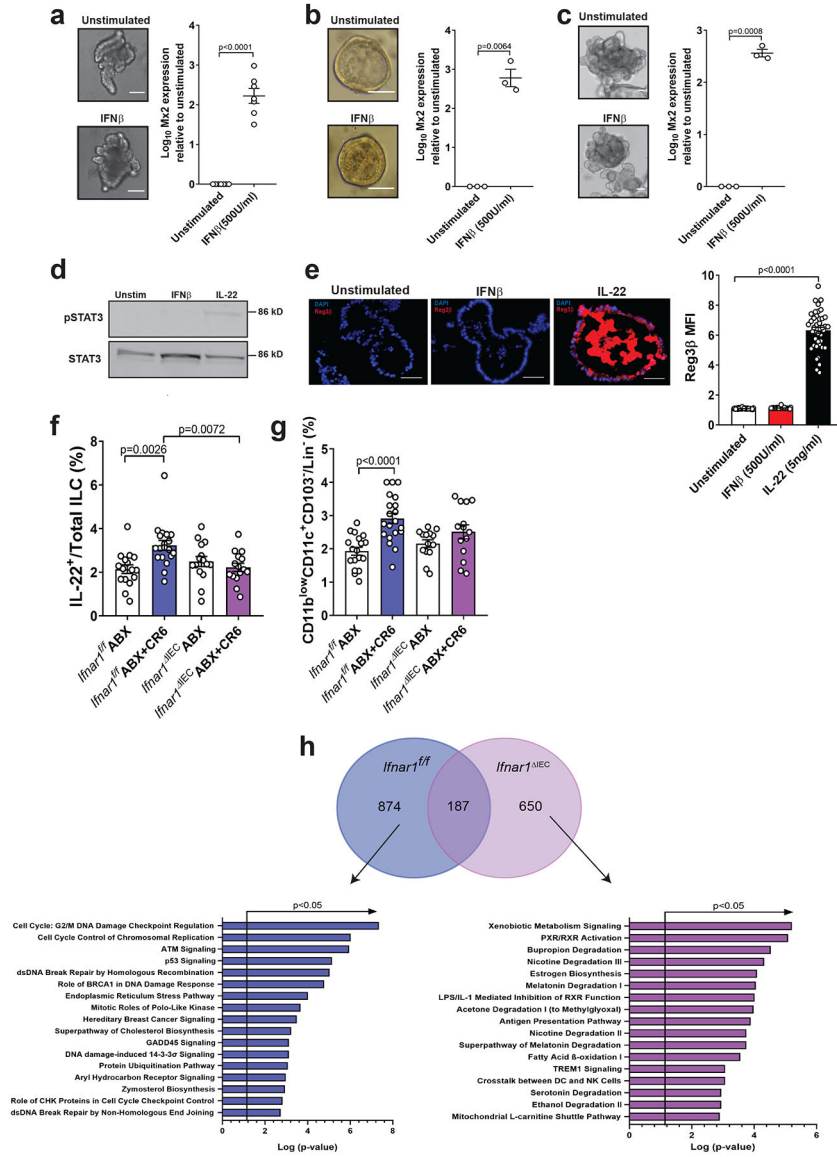


Figure 6: IECs react to IFN-I stimulation and promote an IL-22 response.

Representative images of murine SI (a), murine colon (b) or human colon (c) organoids either unstimulated or stimulated with 500U/ml of IFNβ for 48 h and expression of *Mx2* mRNA relative to unstimulated organoids. Scale bars represent 50μM. The following number of independent experiments were performed: (a), n=7; (b), n=3 and (c), n=3. Log₁₀ transformed *Mx2* expression was analyzed by two-tailed paired t-test. (d) Phosphorylation of STAT3 at 2 h in SI organoids. Representative of 4 independent experiments. (e) Representative images of Reg3β expression and representative mean fluorescence intensity (MFI) of individual organoids of 2 independent experiments at 24 h. Scale bars represent 50μM. The following number of organoids were analyzed: unstimulated, n=34; IFNβ, n=32 and IL-22, n=40. ANOVA with Dunnett’s multiple comparisons test was used to analyze Reg3β expression. Proportion of IL-22 expressing ILC (f) and CD11b^{low}CD11c⁺CD103⁻ cells (g) in ABX-treated *Ifnar1^{ff}* and *Ifnar1^{IEC}* mice at day 6 post DSS. The following

number of mice were analyzed for IL-22: *Ifnar1^{fl/fl}* ABX, n=16; *Ifnar1^{fl/fl}* ABX+CR6, n=19; *Ifnar1^{IEC}* ABX, n=15 and *Ifnar1^{IEC}* ABX+CR6, n=15. The following number of mice were analyzed for CD11b^{low}CD11c⁺CD103⁻ cells: *Ifnar1^{fl/fl}* ABX, n=18; *Ifnar1^{fl/fl}* ABX+CR6, n=20; *Ifnar1^{IEC}* ABX, n=14 and *Ifnar1^{IEC}* ABX+CR6, n=14. ANOVA with Tukey's multiple comparisons test was used to analyze cell populations. (h) Gene expression analysis of IECs from MNV CR6-infected *Ifnar1^{fl/fl}* (n=3) and *Ifnar1^{IEC}* (n=3) mice compared to uninfected mice (*Ifnar1^{fl/fl}*, n=3 and *Ifnar1^{IEC}*, n=3) at day 6 post DSS. Circles in Venn diagram represent number of transcripts that are enriched following MNV-infection in the mice with the indicated genotypes. Pathway analysis was performed on the non-overlapping gene set and p-values determined by Ingenuity Pathway Analysis. All bars represent mean and error bars represent standard error of the mean. All p-values are shown in the figure.

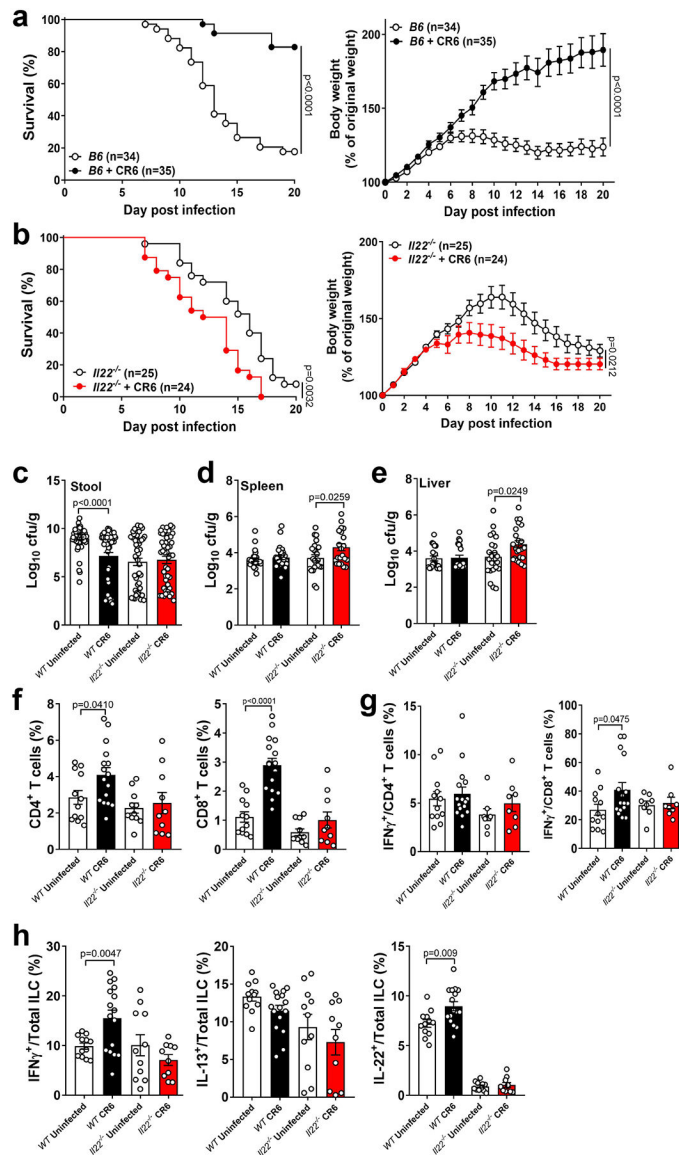


Figure 7: MNV protects young mice from enteric bacterial infection.

Survival and weights of *B6* (a) and *Il22*^{-/-} (b) mice infected with *C. rodentium* at 21 days old. Survival curves were analyzed using the log-rank Mantel–Cox test. For weight curves, AUC was determined for each mouse and difference between uninfected and CR6-infected groups determined by two-tailed t-test. Mean and standard error of the mean is shown for weight analysis. Bacterial titers in the stool (c), spleen (d) and liver (e) at 6 dpi with *C. rodentium*. The following number of mice were analyzed in (c): *WT* Uninfected, n=56; *WT* CR6, n=59; *Il22*^{-/-} Uninfected, n=48 and *Il22*^{-/-} CR6, n=47. The following number of mice were analyzed in (d): *WT* Uninfected, n=25; *WT* CR6, n=29; *Il22*^{-/-} Uninfected, n=24 and *Il22*^{-/-} CR6, n=22. The following number of mice were analyzed in (e): *WT* Uninfected, n=19; *WT* CR6, n=21; *Il22*^{-/-} Uninfected, n=23 and *Il22*^{-/-} CR6, n=23. (f) Proportion of colonic CD4⁺ and CD8⁺ T cells. (g) Proportion of colonic CD4⁺ and CD8⁺ T cells expressing IFN γ . (h) Proportion of IFN γ ⁺, IL-13⁺ and IL-22⁺ cells in the colonic ILC

population. The following number of mice were analyzed for cell proportions: *WT* Uninfected, n=12; *WT* CR6, n=16; *II22*^{-/-} Uninfected, n=11 and *II22*^{-/-} CR6, n=10. Log₁₀ transformed bacterial titers and cell proportions were analyzed using two-tailed t-tests. All bars represent mean and error bars represent standard error of the mean. All p-values are shown in the figure.